

PIV measurement of roof corner vortices

Kyung Chun Kim[†], Ho Seong Ji[‡] and Seung Hak Seong^{‡†}

*School of Mechanical Engineering, Pusan National University, San 30, Jangjeon-Dong,
Kumjung-Ku, Pusan 609-735, Korea*

Abstract. Conical vortices on roof corners of a prismatic low-rise building have been investigated by using the PIV (Particle Image Velocimetry) technique. The Reynolds number based on the free stream velocity and model height was 5.3×10^3 . Mean and instantaneous vector fields for velocity, vorticity, and turbulent kinetic energy were measured at two vertical planes and for two different flow angles of 30° and 45° . The measurements provided a clear view of the complex flow structures on roof corners such as a pair of counter rotating conical vortices, secondary vortices, and tertiary vortices. They also enabled accurate and easy measurement of the size of vortices. Additionally, we could easily locate the centers of the vortices from the ensemble averaged velocity fields. It was observed that the flow angle of a 30° produces a higher level of vorticity and turbulent kinetic energy in one of the pair of vortices than does the 45° flow angle.

Key words: PIV (Particle Image Velocimetry); conical vortices; wind tunnel measurement; instantaneous and ensemble averaged velocity; vorticity and turbulent kinetic energy.

1. Introduction

Low-rise buildings, having common features of sharp edges, ridges, and rectangular shape, are often subjected to conical vortices at their corners as well as flow separations from the sharp edges. Effects of the vortices can be significant to local wind loading particularly in roof corners where severe damage by winds are frequently observed. Extensive research on the wind load around low-rise buildings have been conducted over the past two decades. In recent years, the wind tunnel modeling technique on low-rise buildings has been greatly advanced by some research groups. One is the CSU/TTU wind engineering group who center on a prismatic low-rise experimental building at Texas Tech University (TTU) (Cochran and Cermak 1992, Bienkiewicz and Yawei 1992, Ham and Bienkiwicz 1998). Modeling the overall wind conditions on the TTU building in a wind tunnel seems to be quite successful in making a fairly correct estimation of full-scale loadings. The main problem in modeling has been with roof corners under the influence of the conical vortices. These areas show large amplitude excursions in surface-pressure fluctuations. Modeling was not successful in a wind tunnel. Most researchers agree that pressure fluctuations with such excursions may be due to the vortex flow above the surfaces of the roof. Tieleman *et al.* (1996) compared surface pressures for the full-scale and model-scale TTU building. They suggested that mismatching peak pressures in

[†] Professor, Corresponding Author

[‡] Graduate Student

^{‡†} Assistant Professor

the region of flow separation and reattachment on a roof corners for the oblique flow angles may be due the lack of sufficient turbulence intensity in a lateral direction. To explore flow structures in corners, correlations between the roof vortex and the roof pressure was investigated by the conventional measurement and flow visualization technique (Bank *et al.* 2000).

Other groups who have studied roof flow include Marwood and Wood (1997) and Kawai and Nishimura (1996). Kawai (2000) demonstrated that the most significant peak pressures are triggered when the flow direction is 20~30 degrees in a square shape model. Flow structures of the conical vortices were obtained by hot wire measurement. However, instantaneous flow fields could not be obtained because of the limitations with the hot wire measurement. Hwangbo *et al.* (2000) investigated similar characteristics between mean and rms pressure distribution on the roof of a 1:50 scaled TTU building model. They confirmed the effects of wind direction on surface pressure distribution.

Recently, the PIV technique has emerged as a powerful tool to provide easy access to rich informations on the complex flows (Kim *et al.* 2000). It is also a useful tool for wind engineering and industrial aerodynamics applications. In this study, quantitative flow is measured using the PIV technique in order to investigate the conical vortices. The capability of measuring instantaneous flow fields provides a better understanding of unsteady motions of roof corner vortices. Physical insights are also gained as to the occurrence of the peak suction pressure at a certain flow angles. The structure of the corner vortices can be further explained from the vorticity and turbulent kinetic energy (TKE) distributions.

2. Experimental apparatus and methods

2.1. Experimental setup

Measurements were conducted using a blow-down type of open circuit wind tunnel at Pusan National University. The wind tunnel has a test section of $0.8\text{ m} \times 0.3\text{ m} \times 2\text{ m}$ ($W \times H \times 3L$) and a contraction area ratio of 2.67:1. The 1:92 scaled TTU model has a dimension of $140\text{ mm} \times 95\text{ mm} \times 40\text{ mm}$ ($L \times W \times H$). The model building and floor are made of glass to minimize reflection of laser sheet beam. Fig. 1 shows a schematic diagram of the experimental setup. The free stream velocity was fixed to be $U_\infty = 2\text{ m/s}$, and the Reynolds number (Re_H) based on the model height was 5.3×10^3 . The model was located 1 m downstream from the test section entrance. The experiment was performed for two flow angles 30° and 45° . The laser beam illuminated the plane perpendicular to the flow and the model roof using a cylindrical lens located above the test section. The CCD camera was aligned so as to be perpendicular to the laser sheet planes as shown in Fig. 1.

2.2. Experimental methods

The PIV system used for this study is composed of an Nd-Yag Laser system, a high resolution CCD camera, a synchronizer (TSI 610032), and a personal computer. The laser for the light source is a double pulsed type and the maximum energy is 250 mJ per pulse. The beam is expanded into a thin light sheet (about 1 mm thick) through a convex cylindrical lens with a very short focal length (-50 mm). For image capturing, the PIVCAM 10-15 CCD camera was used which has a pixel resolution of $1\text{K} \times 1\text{K}$. The time interval (Δt) between two successive frames was 200 μs . The CCD camera lens for this study had a Nikon telephotographic lens (105 mm) to provide a $9\text{ cm} \times 9\text{ cm}$

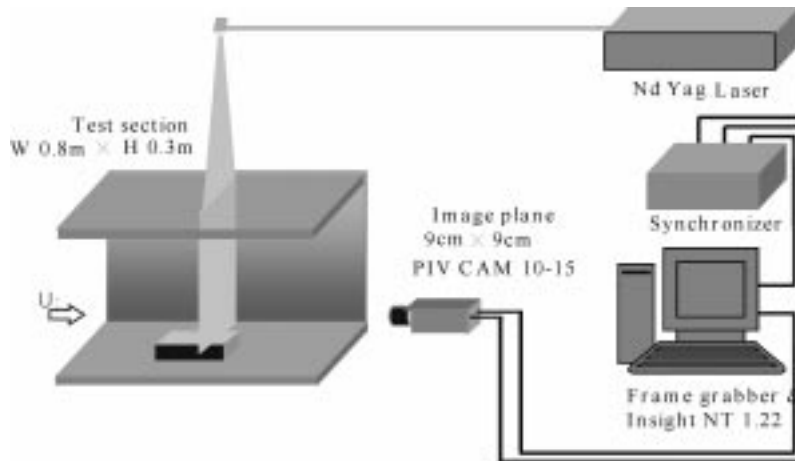


Fig. 1 Schematic diagram of experimental setup

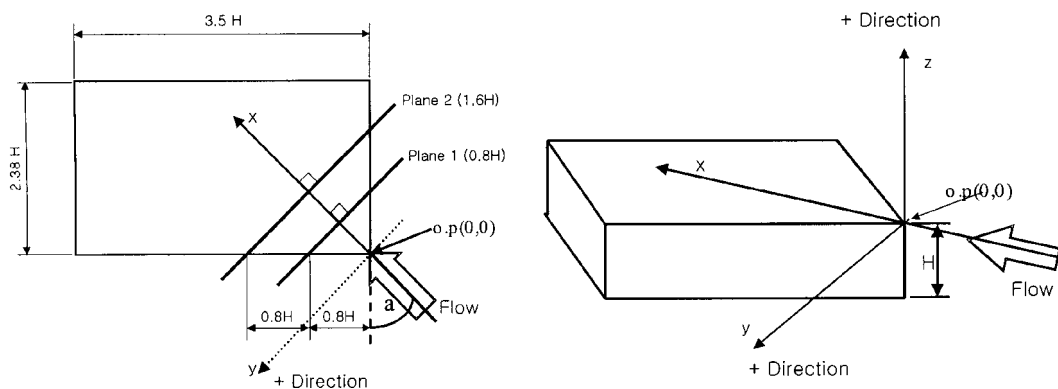


Fig. 2 Measurement positions, angle of attack definition and coordinate system

field of view. The seeding particles were olive oil aerosol which is generated by the home-made Laskin nozzle. The nominal diameter of seeding particles is $2\ \mu\text{m}$, and the scattered lights correspond to 2~4 pixels of image. The PIV-ACE V1.0 developed by Applied Fluid Laboratory at Pusan National University was used for interrogation, post processing, and velocity vector calculation based on the two frame cross - correlation method with a sub-pixel enhancement algorithm.

The size of the interrogation window was selected as 24×24 pixels. Fifty percent of overlap was permitted. A total of 6,889 velocity vectors were interrogated, hence the spatial resolution of the velocity data was 1.08 mm. After removing spurious vectors, ensemble averaging and other statistical calculations were carried out by using a post processing program (PIV-ACE V1.0). For each case, 400 image frames (200 velocity fields) were captured and processed.

Fig. 2 shows the measurement positions, the flow angle, and the measurement coordinate system. The CCD camera is located at the downstream side and aligned with the flow direction passing the origin.

3. Results and discussion

3.1. Approaching boundary layer

The approaching boundary layer was measured at 1m downstream from the test section entrance by using the PIV technique. The mean velocity and turbulent intensity profiles are presented in Fig. 3. The free stream turbulent intensity is about 1% and the peak local intensity is about 2.5%, which seems much smaller than a fully developed turbulent boundary layer value. Since we didn't use any boundary layer tripping wire and the glass plate is smooth enough, the approaching boundary layer at the model position can be thought of as a laminar flow. It can be conjectured that the local Reynolds number, $Re_x = 1.39 \times 10^5$ is less than the critical Reynolds number ($\approx 5 \times 10^5$), and the Reynolds number based on the boundary layer thickness ($\delta = 12.4$ mm) is $Re_\delta = 1.73 \times 10^3$. The displacement thickness (δ^*) and the momentum thickness (Θ) are estimated as 2.78 mm and 1.35 mm, respectively. The calculated shape factor (δ^* / Θ) has the value of 2.06 which is less than that of the laminar flat plate, 2.59. These results indicate that there exists a transitional nature in the approaching boundary layer. Since the height of the building model is much higher than the approaching boundary layer thickness, the separation due to model can be classified into the overwhelming perturbation regime (Bradshaw 1972). Therefore, the separated flow wake behind the model might be different compared to the actual building submerged in a thick atmospheric boundary layer.

3.2. Ensemble averaged velocity field

The images for velocity fields were captured at locations where the structure of the conical vortices and the angles could be investigated as clearly as possible, as shown in Fig. 9.

Fig. 4 shows the mean velocity vector field taken at the 0.8H location for the case of a 30° wind direction. The mean velocity field was obtained by an ensemble averaging over the 200 instantaneous flow fields. Since the CCD camera axis and the flow direction did not coincide with each other (see

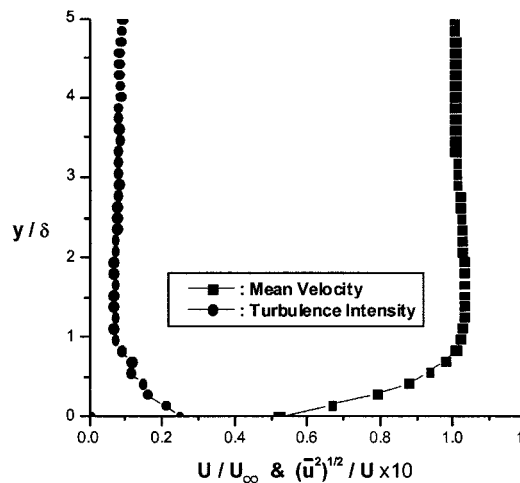


Fig. 3 Approaching boundary layer profile

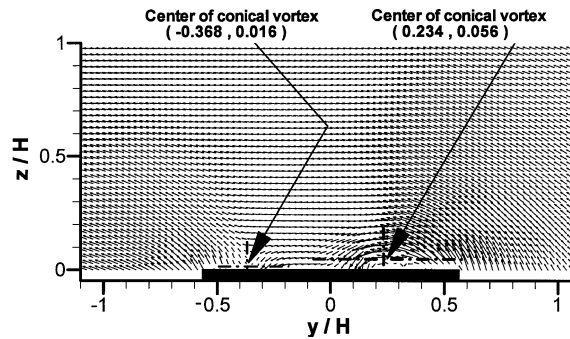


Fig. 4 Mean flow profile
(Angle of attack : 30° / Measurement position : $0.8H$)

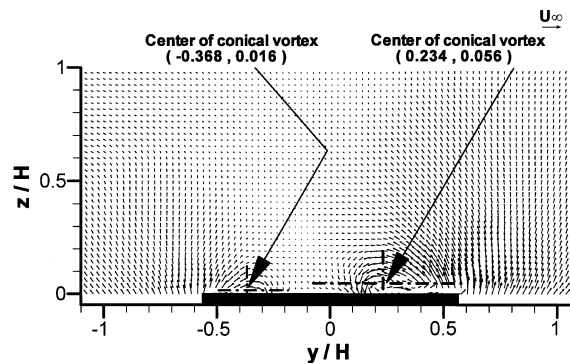


Fig. 5 Mean flow profile ($V+0.3V$)
(Angle of attack : 30° / Measurement position : $0.8H$)

Fig. 9(a)), there is a uniform side flow in the free stream region. It is difficult to find a clear formation of the corner vortex especially at the corner in the negative y direction.

A Galilian transformation has been applied to remove uniform velocity components in the laser sheet plane due to the angle between the flow direction and the angle of view in Fig. 9(a). The transformation can be done simply adding $0.3V$ to the original velocity vector field. The $0.3V$ was obtained based on the velocity field data which made the free stream velocity at the plane almost zero. In Fig. 5, on the vertical plane perpendicular to the approaching flow, two counter rotating vortices with different sizes are clearly observed. The centers of the conical vortices at the y - z plane are found to be around $(0.234H, 0.056H)$ and $(-0.368H, 0.016H)$, respectively. The center locations were approximately identified because they were based on the velocity profile plot. Due to the oblique approaching flow angle, the vortex on the right corner looks better developed with an aid of the large scale flow separation along the edge and bigger than that on the left corner. Note that the magnitude of vertical velocity near the right corner exceeds the free stream value. The high transverse velocity near the corner may play a significant role in inducing peak suction pressure, as discussed in many previous studies.

In Fig. 6, on the plane at $1.6H$, the vortices become bigger and further developed. Their centers were raised to $(0.454H, 0.118H)$ and $(-0.749H, 0.034H)$, respectively. In the mean velocity field, the

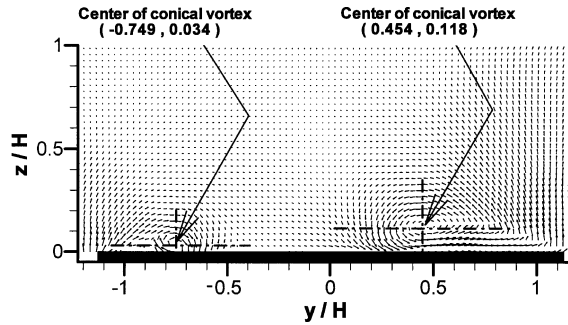


Fig. 6 Mean flow profile ($V+0.3V$)
(Angle of attack : 30° / Measurement position : $1.6H$)

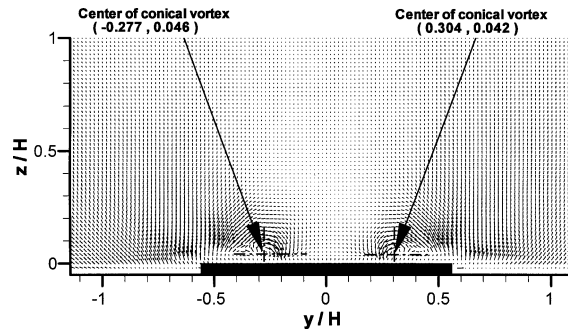


Fig. 7 Mean flow profile
(Angle of attack : 45° / Measurement position : $0.8H$)

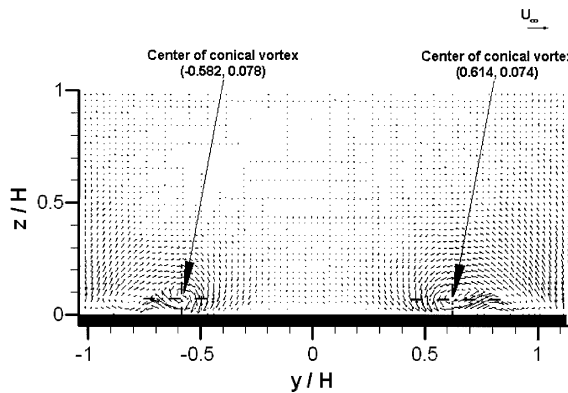


Fig. 8 Mean flow profile
(Angle of attack : 45° / Measurement position : $1.6H$)

secondary vortices are not clearly seen. Although the secondary vortices are being developed, the magnitude of the velocity associated with the vortices turn out smaller than the free stream value.

Figs. 7 and 8 show the mean velocity fields in the case of a 45° angle of attack at the $0.8H$ and $1.6H$ planes, respectively. In this case, any velocity shift is not necessary since the camera is aligned

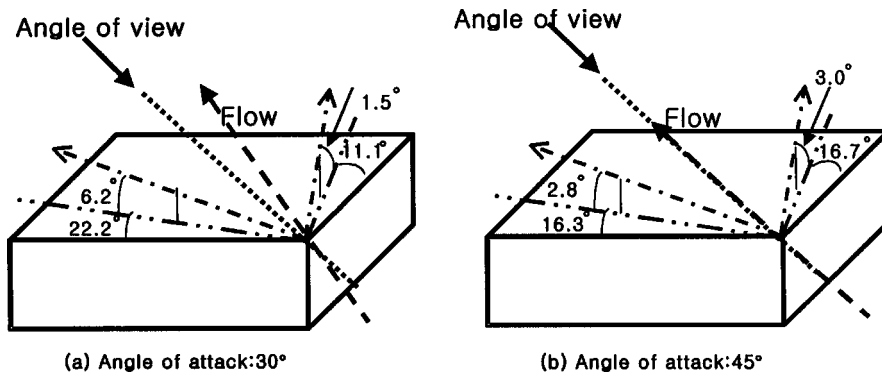


Fig. 9 Centers of conical vortices

with the flow direction. In Fig. 7, the magnitudes and the locations of the conical vortices show quite a good symmetric nature, but are not perfectly symmetric. This means that the shape of a roof, which is not a square but a rectangular shape with a wider side, also affects the generation of the conical vortices and the evolutions.

The conical vortices in the vertical plane of $0.8H$ have center positions at $(0.304H, 0.042H)$ and $(-0.277H, 0.046H)$, respectively. The magnitude of vertical velocity near the corner seems less than that of the free stream. Hence, the peak suction pressure might be less than the case of the 30° angle of attack. At the $1.6H$ plane in Fig. 8, the centers of conical vortices have been changed and the sizes of the conical vortices have been enlarged in comparison with the $0.8H$ plane. The vortices still preserve their symmetric structures with centers at $(0.614H, 0.074H)$ and $(-0.582H, 0.078H)$. At the $1.6H$ plane, the secondary vortex can be seen in the ensemble averaged velocity field.

The conical vortices being generated at the edge are caused by flow separation from the building's edges at the corner regions. The axis of the conical vortices are inclined with respect to the edges of the corners. From the measurement of the ensemble averaged velocity field, the center lines of the conical vortices can be drawn as shown in Fig. 9. With the assumption that a corner vortex has a conical shape, the center axis is estimated by simply connecting the center of the main conical vortex and the apex of the corner. As expected in Fig. 9, from the upstream point of view, the vortex in the left-hand side is shown to be bigger than that in the right. In the case of a 30° angle of attack, the angle between the roof edge and the axis of the vortex in the left is bigger than that of right because of the asymmetric flow direction. The horizontal angle of the vortex axis on the left-hand side is about 22.2° , and that of the vortex on the right is about 11.1° in the horizontal plane. The vertical angles of the conical vortices are 6.2° on the left-hand side and 1.5° on the right-hand side, which are estimated in the same way as the horizontal angles.

The results demonstrate that the size of the windward vortex is more than twice that of the leeward vortex. Because of the large momentum converted to the vortex motion from the free stream, relatively high suction pressure can be expected at the left-hand side. This conjecture is supported by the many previous pressure measurement studies including Hwangbo *et al.* (2000) in which the peak mean and rms pressure coefficients were observed at the left corner at the 30° angle of attack.

For the case of a 45° , expected results were revealed. The axes of the vortices are located at nearly the same angle (around 16.5°) in the horizontal plane from the two edges. The slight

difference of the angle, 0.4° , as illustrated in Fig. 9, is due to the fact that the model is not exactly a square (symmetric) shape. The vertical inclination angle is about 3.0° , and nearly the same for the conical vortices on both sides.

In the TTU observation data from the flow visualization, the vortex core angles were 9° , 13° , and 19° for the wind directions at 30° , 45° , and 60° respectively (Banks *et al.* 2000). Our results (11.1° , 16.7° , and 22.2°) show consistently higher angles compared with the full scale data. The difference may be due to the lower Reynolds number and the thin approaching boundary layer. Similar trends were observed in data from averaged velocity fields in smooth flow (Stathopoulos *et al.* 1999), in which the vortex core angles were 11° , 18° and 23° for wind directions 30° , 45° and 60° , respectively. These values are in agreement with our results.

3.3. Instantaneous velocity field

Figs. 10 and 11 show the instantaneous velocity vector fields captured on the same plane but for different realizations. The vortex centered at $(0.498H, 0.123H)$ in Fig. 10 has moved to $(0.434H, 0.101H)$ in Fig. 11. The movement of the vortex centers indicates that there exists a swaying motion, but the motion is not so severe. The swaying was also observed by Kawai and Nishimura

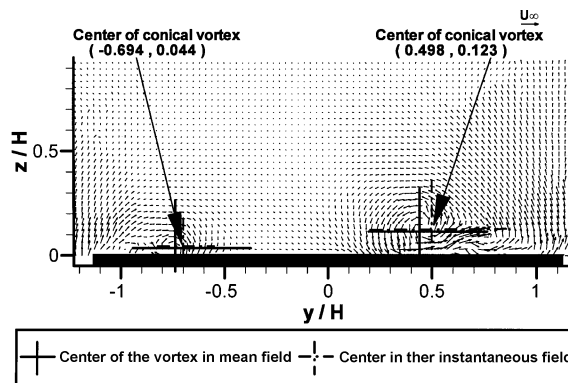


Fig. 10 Instantaneous flow field ($V+0.3V$)
(Angle of attack : 30° / Measurement position : $1.6H$)

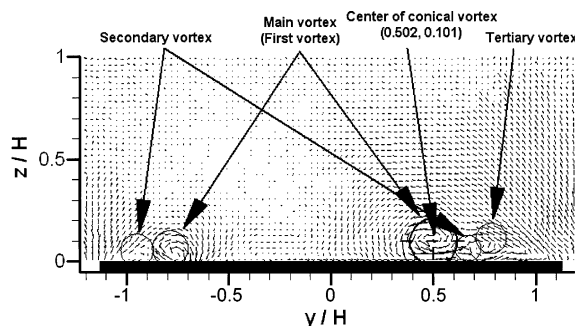


Fig. 11 Instantaneous flow field ($V+0.3V$)
(Angle of attack : 30° / Measurement position : $1.6H$)

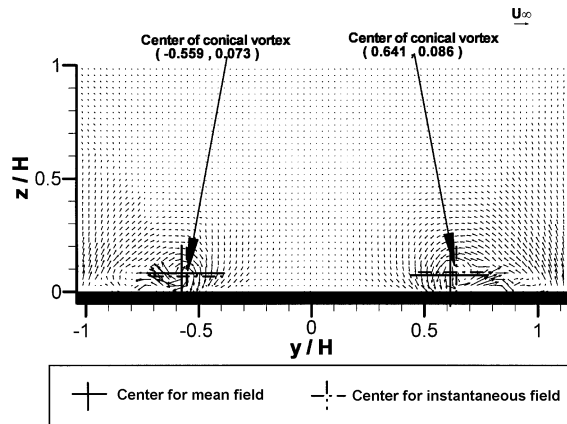


Fig. 12 Instantaneous flow field
(Angle of attack : 45° / Measurement position : $1.6H$)

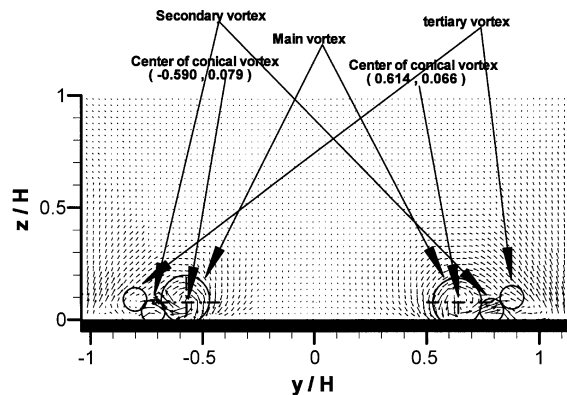


Fig. 13 Instantaneous flow field
(Angle of attack : 45° / Measurement position : $1.6H$)

(1996) and some other researcher. In Fig. 11, the secondary vortex is clearly observed near the main vortex. A new vortex is also observed near the secondary vortex. So far, only the existence of the main and secondary vortex has been reported in the open literature. Our instantaneous PIV results show the existence of the third new vortex. The secondary vortex has a counter-rotating direction to the main vortex. The new vortex has the same rotating direction as the main vortex but a counter-rotating direction to the secondary vortex. The new vortex is therefore formed by the secondary vortex and the large scale flow which is separated from the roof edge. The reattachment of the separated shear layer from the main vortex stream near the surface creates the secondary vortex. The structure of the tertiary vortex including intensity and direction of rotation can be more clearly seen in the vorticity fields in Figs. 14~17.

Figs. 12 and 13 show the instantaneous velocity fields for the 45° wind direction. The figures reveal similar information about the detail in flow structures including the secondary vortex, the tertiary vortex, and evidence of swaying in the axes of the vortices.

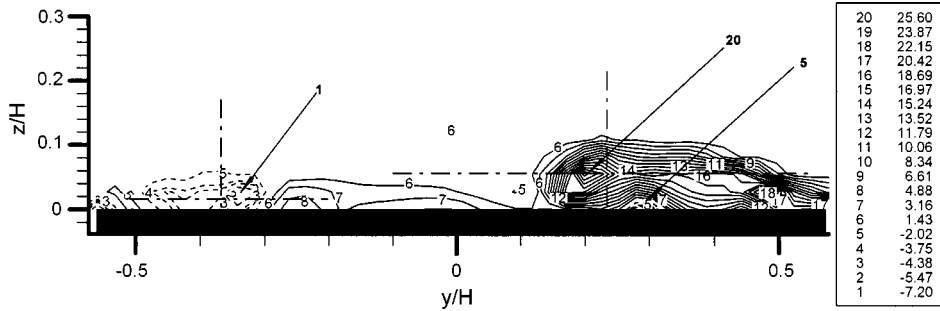


Fig. 14 Vorticity field
(Angle of attack : 30° / Measurement position : 0.8H)

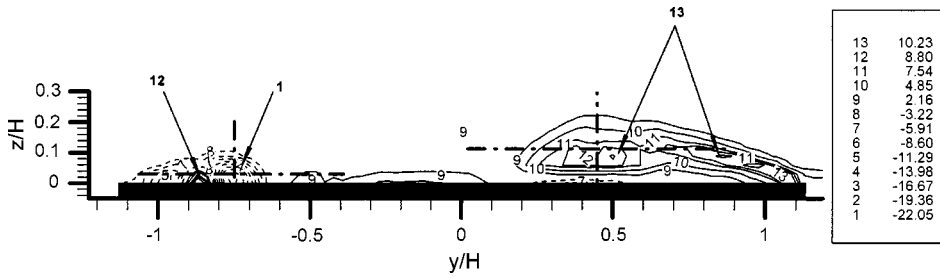


Fig. 15 Vorticity field
(Angle of Attack : 30° / Measurement position : 1.6H)

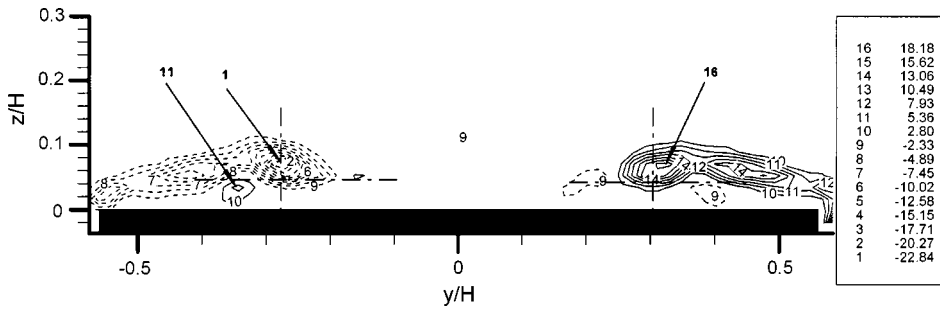


Fig. 16 Vorticity field
(Angle of attack : 45° / Measurement position : 0.8H)

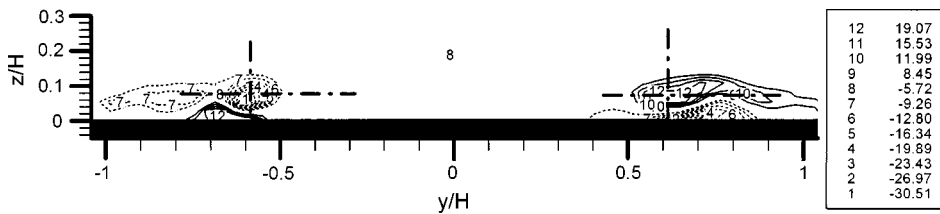


Fig. 17 Vorticity Field
(Angle of attack : 45° / Measurement position : 1.6H)

3.4. Vorticity and turbulent kinetic energy field

The streamwise vorticity fields are deduced from the measured velocity gradients using Eq. (1).

$$\omega_x = \frac{\partial w}{\partial y} - \frac{\partial v}{\partial z} \quad (1)$$

The normalized vorticity ($\omega_x \bullet H / U_\infty$) contours illustrate the strengths and shapes of the conical vortices. Figs. 14 and 15 show the mean vorticity fields for the case of a 30° flow direction. At the position of 0.8H, a large positive vorticity (counter-clockwise rotation) region appears on the right-hand side, while small negative vorticity contours appear on in the left-hand side. One should note that the peak value of the counter-clockwise vorticity is three and a half times higher than that of the clockwise vorticity. One can see that the peak vorticity occurs near the center of vortex motion which was estimated from the velocity field.

The vorticity contour profile in the right-hand side vortex in Fig. 14 demonstrates the existence of three vortical motions. Two positive peaks are present. One is near the center of the main vortex. The other is found near $y / H = 0.5$ which represents the existence of the tertiary vortex motion. The negative value of the streamwise vorticity observed between the main and tertiary vortex is attributed to the secondary vortex.

As the fluid proceeds downstream, the two conical vortices at both edges develop in a different way as can be seen in Fig. 15. The left-hand side vortex becomes much stronger, while the right-hand side vortex decreases in strength. As expected, both shape of the vortices have become larger. Evidence of three vortical motions seems quite apparent in the right-hand side conical vortex. However, the left-hand side vortex has mostly positive vorticity values and a relatively smaller clockwise vorticity near the wall. This feature is well reflected in the ensemble averaged velocity field in Fig. 6. The strong rotational moment in the counter-clockwise direction from the windward edge influences the development of the secondary vortex. The growth of the secondary vortex in size and strength in the leeward side 1.6H plane might be possible due to the center movement and relatively weak momentum of the main vortex in the clockwise direction.

Figs. 16 and 17 depict the streamwise vorticity plots at the 0.8H and 1.6H planes in the case of a 45° flow respectively. Almost symmetric distributions of vorticity with opposite signs are seen clearly at the 0.8H location as shown in Fig. 16. The existence of three vortical motions can be found easily in the two negative and one positive vorticity zones. The location of the peak vorticity value in the main vortical motion coincide roughly with the center of the vortex. The symmetry of the vorticity contour is found to be imperfect.

The slight symmetry differences in size and magnitude are apparent in Fig. 17. The right-hand side vortex is a bit bigger than that of the left-hand side. Noting that the model is not a square, the right-hand side vortex interacts with a wider roof edge than the left-hand side. The difference can be explained. The wider solid wall seems to affect the conical vortex to form a more stable conical shape. The most striking feature is that the secondary vortex develops significantly with downstream movement. The absolute value of the peak vorticity in the secondary vortex turns out to be comparable with that of the main vortex. This common feature of the secondary vortex growth is also observed in the case of the 30° flow. In summary, typical conical vortices on a roof corner appear to consist of three different streamwise vortical motions. The development of the secondary vortex appears to be highly dependent upon the structure of the main vortical motion. The center movement of the main vortex and consequently the weaker linear momentum by the vortex near the surface seem to

foster the secondary vortex development.

The ensemble averaged turbulent kinetic energy distribution gives us dynamic information about the roof corner vortices, since it is caused by the swaying motion and/or turbulent fluctuating behavior of the vortices. The TKE can be deduced from the instantaneous fluctuating velocity fields which are obtained by subtracting the ensemble averaged field from each realization. We did not measure the streamwise velocity fluctuations, hence the TKE distributions were obtained by using the Eq. (2).

$$\bar{q}^2 = \frac{1}{2}(\bar{u}^2 + \bar{v}^2 + \bar{w}^2) = \frac{3}{4}(\bar{v}^2 + \bar{w}^2) \tag{2}$$

where, \bar{u}^2 is assumed to be $0.5(\bar{v}^2 + \bar{w}^2)$.

Figs. 18 and 19 show the contour plot of the TKE distribution at the 0.8H and 1.6H planes a 30° flow direction, respectively. The values of \bar{q}^2 were normalized with U_∞^2 . The formation of a strong conical vortex at the right-hand side in Fig. 18 generates a high level of fluctuating energy which is nearly 27% of the mean velocity kinetic energy. The result supports physical reasons associated with the generation of the spike-like suction pressure near the edge when the angle of attack is within 20°~30° (Kawai 2000).

At the location of 1.6H, a relatively small amount of TKE appear in the left hand side which is produced by vortex motion. On the other hand, the vortex in the right-hand side keeps its turbulent nature continuously, showing that the peak TKE occurs at the region where the three vortical motions interact with each other.

Although the mean velocity fields show symmetric features, the TKE distribution depicts an

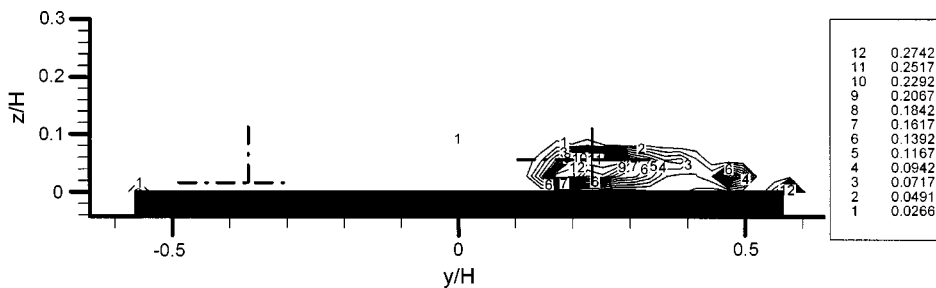


Fig. 18 Turbulent kinetic energy
(Angle of attack : 30° / Measurement position : 0.8H)

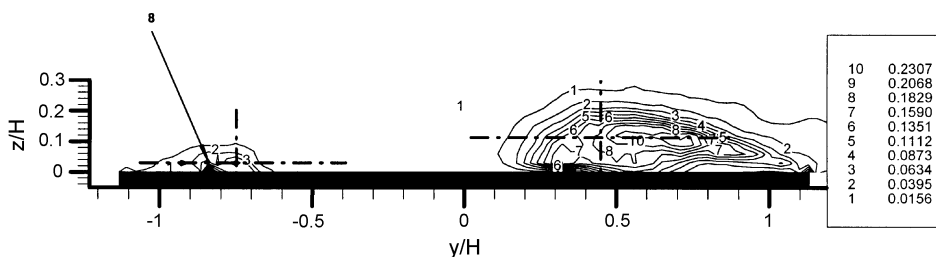


Fig. 19 Turbulent kinetic energy
(Angle of attack : 30° / Measurement position : 1.6H)

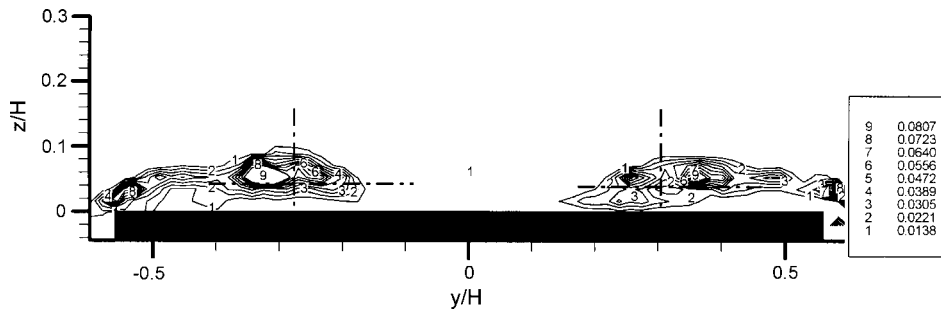


Fig. 20 Turbulent kinetic energy
(Angle of attack : 45° / Measurement position : $0.8H$)

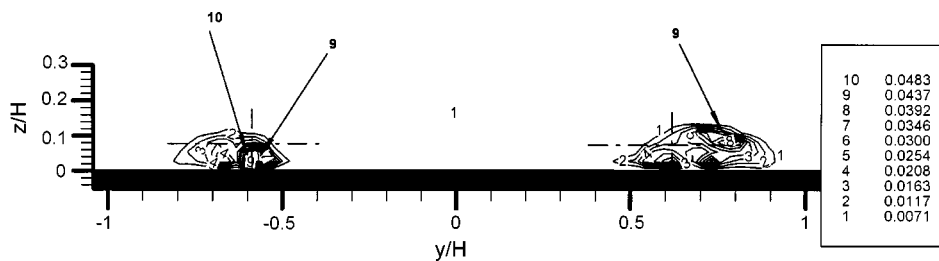


Fig. 21 Turbulent kinetic energy
(Angle of attack : 45° / Measurement position : $1.6H$)

asymmetric nature in the case of a 45° angle (Figs. 20 and 21). In general, the value of a normalized TKE at a 45° angle of attack is found to be 8% of mean flow energy. It is much lower than a 30° angle of attack. This nature is quite reasonable if we remember that the mean and rms values of surface pressure fluctuations for the 308 wind was higher than those of the 45° wind reported in the previous study (Hwangbo *et al.* 2000 and Kawai 2000).

In Fig. 20, the overall TKE distribution in the $0.8H$ plane seems to be symmetric like the vorticity, however the peak level and distribution of the TKE are shown to be different in each vortex.

Such differences and asymmetry appear to be amplified in the $1.6H$ plane of Fig. 21. The TKE seems to be concentrated near the main vortex on the left-hand side vortex flow, while another peak value appears near the wall on the right-hand side. The peak value related with the primary vortex might be caused by a swaying motion. However, the high turbulent energy near the wall corresponds to the turbulent energy production from the solid wall boundary. This evidence is not sufficient to explain the differences in TKE distribution for the case of 45° angle of attack but is consistent with the difference observed in the vorticity distribution.

4. Conclusions

For symmetric and asymmetric flows, the conical vortices on a roof corner have been investigated from PIV measurements. Clear views and rich information on the vortex structures have been obtained by measuring the instantaneous and mean velocity, vorticity, and TKE fields.

In the vorticity field, the new tertiary vortex has been identified which is formed by the secondary

vortex and the separated shear layer from the roof edge. The secondary vortex development has been observed to be significant. At the location about 1.6H, the vorticity of the secondary vortex becomes almost the same as the main vortex. For the symmetric flow, the effects of the asymmetric shape of the model building appear negligible in the velocity fields. However, the effects become appreciable in the vorticity and TKE distributions. The estimated vortex core angles in the horizontal plane have higher values compared with the full-scale data. This difference may be due to the effects of the low Reynolds number and the approaching boundary layer flow condition.

Acknowledgement

This work has been partially supported by the Brain Korea 21 Project.

References

- Bienkiewicz, B. and Sun, Y. (1992), "Local wind loading on the roof of a low-rise building", *J. Wind Eng. Ind. Aerod.*, **45**, 11-24.
- Banks, D., Meroney, R.N., Sarkar, P.P., Zhao, Z. and Wu, F. (2000), "Flow visualization of conical vortices on flat roofs with simultaneous surface pressure measurement", *J. Wind. Eng. Ind. Aerod.*, **84**, 65-85.
- Bradshaw, P. and Wong, F.Y.F. (1972), "The reattachment and relaxation of a turbulent shear layer", *J. Fluid Mech.*, **52**, 113.
- Hwangbo, D., Ji, H.S., Seong, S.H. and Kim, K.C. (2000), "Wind tunnel modeling of prismatic low-rise building in the atmospheric boundary layer", *1st Int. Symp. on Wind and Structure*, 327-336.
- Ham, H.J. Bienkiewicz, B. (1998), "Wind tunnel simulation of TTU flow and building roof pressure", *J. Wind. Eng. Ind. Aerod.*, **77&78**, 119-133.
- Kawai, H. and Nishimura, G. (1996), "Characteristics of fluctuating suction and conical vortices in a flat roof in oblique flow", *J. Wind Eng. Ind. Aerod.*, **60**, 211-225.
- Kawai, H. (2000), "Local peak pressure on a flat roof - mechanism and reduction-", *1st Int. Symp. on Wind and Structures*, 91-98.
- Kim, K.C. (2000), Personal Communications.
- Kim, K.C., Kim, S.K. and Yoon, S.Y. (2000), "PIV measurements of the flow and turbulent characteristics of a round jet in crossflow", *J. of Visualization*, 3(2).
- Marwood, R. and Wood, C.J. (1997), "Conical vortex movement and its effect on roof pressures", *J. Wind. Eng. Ind. Aerod.*, **69&71**, 589-595.
- Stathopoulos, T., Marathe, R. and Wu, H. (1999), "Mean wind pressures on flat roof corner affected by parapets: field and wind tunnel studies", *Eng. Struct.*, **21**, 629-638.
- Tieleman, H.W., Surry, D. and Mehta, K.C. (1996), "Full/model scale comparison of surface pressure on Texas Tech experimental building", *J. Wind. Eng. Ind. Aerod.*, **61**, 1-23.